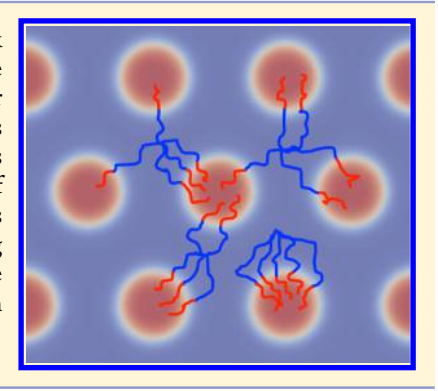
# **Macromolecules**

# Domain Bridging in Thermoplastic Elastomers of Star Block Copolymer

Russell K. W. Spencer\* and Mark W. Matsen\*

Department of Chemical Engineering, Department of Physics & Astronomy, and Waterloo Institute for Nanotechnology, University of Waterloo, Waterloo, Ontario N2L 3G1, Canada

ABSTRACT: The performance of thermoplastic elastomers composed of block copolymers is dependent upon the molecular bridges linking together the discrete minority domains. Here we devise a strategy for calculating the bridging statistics for complex block copolymer architectures, using self-consistent field theory. The method is demonstrated on  $(AB)_M$  stars with M identical diblock arms. The fraction of molecules forming bridges,  $\nu_{\rm b}$ , is found to increase rapidly with M to values well beyond that of conventional ABA triblock copolymers. Once M is of order 10, virtually all molecules form bridges, and furthermore their arms tend to be distributed equally among neighboring minority domains. These high bridging fractions combined with the tendency of single molecules to bridge multiple domains make diblock-arm stars an excellent candidate for improved thermoplastic elastomers.



## **■ INTRODUCTION**

ABA triblock copolymers have been used for thermoplastic elastomers since the 1960s and currently represent the largest sector of the block copolymer industry. These materials are processed in the melt where they self-assemble into an ordered morphology, usually the spherical phase, with the A blocks forming discrete minority domains embedded in a matrix of the B blocks. Cooling the material below the glass or crystallization temperature of the A component locks the A blocks together to form a rubbery network of B blocks.

Naturally, the performance of the elastomer relies on the B blocks bridging between the different discrete A domains. Looped configurations of the B block, where both ends reside on the same A/B interface, do not generally contribute to the elasticity of the material unless the B block happens to be sufficiently entangled with other B blocks. In any case, a high bridging fraction,  $\nu_{\rm b}$ , is desirable. However, bridging is not something that experiments are able to measure, apart from the special case of a lamellar phase,  $^{2,3}$  and so our knowledge of  $\nu_{\rm b}$  is dependent upon theory or simulation. According to selfconsistent field theory (SCFT),  $\nu_b$  in the lamellar, cylindrical, and spherical phases of an ABA triblock copolymer melt is 40-45%, 60–65%, and 75–80%, respectively.<sup>4</sup>

In order to improve the performance of thermoplastic elastomers, researchers have been exploring alternative block copolymer architectures. Much of this has focused on linear ABABA... multiblocks, where the number of repeating blocks is simply increased. 6-9 The multiblocks are generally found to possess better mechanical properties, which is attributed to the difference in their bridging statistics. 10-12 Attention is now turning to more complex architectures. A number of studies have investigated various multibranched architectures, 13-16 some of which have resulted in improved performance. A miktoarm star block copolymer has also received considerable

attention for its superior performance over the linear architectures. 17-19 Our interest, however, is with experi- $\mathrm{ments}^{20-22}$  on  $(\mathrm{AB})_{\mathrm{M}}$  star block copolymers composed of M≥ 3 identical diblock arms, which have likewise demonstrated significant improvement over their linear counterparts (i.e., M =2). Naturally, there will be various contributing factors to these improvements. For instance, the improved performance of the miktoarm star is attributed to larger minority domains of the hard component. In any case, bridging statistics will certainly play an important role, more so for some architectures than

As of yet, there is relatively little understanding regarding the bridging statistics of complex architectures. Hart et al.<sup>23</sup> have used dissipative particle dynamics (DPD) simulations to study comb and star architectures. They found that (AB)<sub>M</sub> stars have an elevated bridging fraction, consistent with the improved performance observed in experiment. 20,22 Unfortunately, due to the computational demands of DPD, this finding was limited to small molecules in the simple lamellar phase. Xu et al.<sup>24</sup> extended the SCFT calculation for the bridging statistics of linear ABA triblocks to that of (AB)<sub>M</sub> stars. They found a dramatic increase in the bridging fraction implying that the stars should exhibit superior elasticity, but unfortunately their calculation is based on a flawed assumption. In this paper, we resolve the problem by developing a new SCFT approach for complex block copolymers architectures. It is then used to evaluate bridging statistic for  $(AB)_M$  stars with M = 2, 3, 5, and 9 arms in the classical lamellar (LAM), cylindrical (CYL), and bcc spherical (SPH) phases.

Received: January 12, 2017 Revised: February 3, 2017 Published: February 16, 2017

# **■ THEORY**

The specific system of our study is a neat melt of n star polymers, each with M identical AB diblock arms joined together by their B ends. The individual arms are modeled as Gaussian chains with N coarse-grained segments, of which a fraction  $f_A$  make up the A block and the rest the B block. Segments are defined based on a common volume,  $\rho_0^{-1}$ , such that the total volume of the melt is  $V = nMN/\rho_0$ , and both A and B segments are assumed to have the same statistical length, a. The incompatibility of unlike segments is controlled by the usual Flory—Huggins parameter,  $\chi$ . This model is then solved using SCFT, <sup>25</sup> which represents the interactions on a  $\gamma$ -type segment at position  $\mathbf{r}$  by the field  $w_{\gamma}(\mathbf{r})$ , where  $\gamma = \mathbf{A}$  and  $\mathbf{B}$ . Note that the molecules and their arms will be treated as if they are distinguishable; the actual indistinguishability will not affect any of the quantities we are calculating.

Before evaluating bridging statistics, we need to first determine the equilibrium morphology (i.e., LAM, CYL, or SPH) along with its self-consistent fields,  $w_{\gamma}(\mathbf{r})$ . To do this, we consider a single diblock arm with its contour parametrized from s=0 at the A end to s=1 at the B end. The (sN)'th segment is then pinned at  $\mathbf{r}$ , which divides the arm into two portions. A partial partition function,  $q(\mathbf{r},s)$ , for the portion with the free end is obtained by starting from  $q(\mathbf{r},0)=1$  and integrating the modified diffusion equation

$$\frac{\partial}{\partial s}q(\mathbf{r},s) = \left[\frac{a^2N}{6}\nabla^2 - w_{\gamma}(\mathbf{r})\right]q(\mathbf{r},s)$$
(1)

forward in s with  $\gamma = A$  for  $s < f_A$  and then  $\gamma = B$  for  $s > f_A$ . The partial partition function,  $q^{\dagger}(\mathbf{r},s)$ , for the other portion is integrated in the negative s direction using the same eq 1, but with the right-hand side multiplied by -1. The fact that its end is attached to M-1 other arms is accounted for by starting from  $q^{\dagger}(\mathbf{r}, 1) = q^{M-1}(\mathbf{r}, 1)$ . The product of the two partial partition functions gives the probability distribution of the (sN)'th segment

$$\rho(\mathbf{r}, s) = Vq(\mathbf{r}, s)q^{\dagger}(\mathbf{r}, s)/Q$$
 (2)

where the normalization factor

$$Q = \int q^{M}(\mathbf{r}, 1) d\mathbf{r}$$
(3)

corresponds to the partition function of an unconstrained star. It then follows that the dimensionless concentrations of A and B segments are

$$\phi_{\mathbf{A}}(\mathbf{r}) = \int_0^{f_{\mathbf{A}}} \rho(\mathbf{r}, s) \, \mathrm{d}s \tag{4}$$

$$\phi_{\mathbf{B}}(\mathbf{r}) = \int_{f_{\mathbf{A}}}^{1} \rho(\mathbf{r}, s) \, \mathrm{d}s$$
 (5)

respectively. Now that the concentrations are known, the fields can be adjusted to satisfy the self-consistent conditions

$$w_{A}(\mathbf{r}) = \chi N \phi_{B}(\mathbf{r}) + \xi(\mathbf{r})$$
(6)

$$w_{\rm B}(\mathbf{r}) = \chi N \phi_{\rm A}(\mathbf{r}) + \xi(\mathbf{r})$$
 (7)

where  $\xi(\mathbf{r})$  is a pressure field that enforces incompressibility,  $\phi_A(\mathbf{r}) + \phi_B(\mathbf{r}) = 1$ . The final step is to minimize the free energy

$$\frac{F}{nk_{\rm B}T} = -\ln Q + \frac{M}{V} \int [\chi N \phi_{\rm A}(\mathbf{r}) \phi_{\rm B}(\mathbf{r}) - w_{\rm A}(\mathbf{r}) \phi_{\rm A}(\mathbf{r}) - w_{\rm B}(\mathbf{r}) \phi_{\rm B}(\mathbf{r})] d\mathbf{r}$$
(8)

with respect to the domain size, *D*, of the morphology. There will be a separate solution for each possible morphology; the equilibrium morphology is the one with the lowest free energy. The numerics for this part of the calculation are performed using the spectral algorithm described in ref 27.

Once the equilibrium morphology is obtained, we can then evaluate the bridging statistics. To facilitate this, the melt is divided into Voronoi cells, each containing a single A domain. For the LAM phase, the cells are parallel planes; for the CYL phase, they are hexagons; for the SPH phase, they are truncated octahedrons. An arm is said to belong to the cell if its AB junction ( $s = f_A$ ) lies in the cell. We focus on one particular Voronoi cell, which we refer to as the first cell. A partial partition function,  $\overline{q}(\mathbf{r},s)$ , for an arm restricted to the first cell is calculated by propagating s forward from

$$\overline{q}(\mathbf{r}, f_{\mathbf{A}}) = \begin{cases} q(\mathbf{r}, f_{\mathbf{A}}), & \text{if } \mathbf{r} \text{ is in the first cell} \\ 0, & \text{otherwise} \end{cases}$$
 (9)

using eq 1. In this case,  $\overline{q}(\mathbf{r},s)$  is not periodic, and thus the diffusion equation needs to be solved in a relatively large volume, but fortunately this only needs to be done once for any given set of system parameters. The numerics for this step are done using the pseudospectral algorithm introduced by Ranjan et al. <sup>28</sup>

Given  $\overline{q}(\mathbf{r},s)$ , the partition function for a single star with its center at  $\mathbf{r}$  and a total of m arms in the first cell can be expressed as

$$Q_{m}(\mathbf{r}) = {M \choose m} \overline{q}^{m}(\mathbf{r}, 1) [q(\mathbf{r}, 1) - \overline{q}(\mathbf{r}, 1)]^{M-m}$$
(10)

The first factor is the number of ways of choosing the m arms from a total of M, the second factor is the partition function for m arms constrained to the first cell, and the last factor is the partition function for M-m arms excluded from the first cell. From this, we obtain the joint distribution

$$P_m(\mathbf{r}) = mQ_m(\mathbf{r})/Q' \tag{11}$$

for the probability that an arm in the first cell belongs to a star with its center at  $\mathbf{r}$  and a total of m arms in the first cell. Thus, the integrated (or marginal) distribution

$$\overline{P}_{m} = \int P_{m}(\mathbf{r}) \, d\mathbf{r} \tag{12}$$

provides the probability that an arm in the first cell belongs to a star with m arms in the first cell. The normalization factor

$$Q' = M \int \overline{q}(\mathbf{r}, 1) q^{M-1}(\mathbf{r}, 1) d\mathbf{r}$$
(13)

in eq 11 corresponds to the partition function of a star with one or more arms in the first cell. One can show, using the binomial theorem, that the normalization gives

$$\sum_{m=1}^{M} \overline{P}_m = 1 \tag{14}$$

Since all the Voronoi cells are equivalent, it follows that the overall fraction of stars that form bridges is

$$\nu_{\rm b} = \sum_{m=1}^{M-1} \overline{P}_m = 1 - \overline{P}_M \tag{15}$$

#### RESULTS

The equilibrium phase behavior of  $(AB)_M$  star blocks is very similar to that of the conventional AB diblock.<sup>29</sup> Figure 1 shows

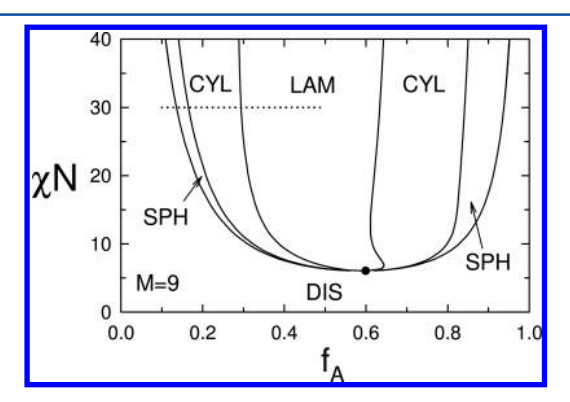


**Figure 1.** Phase diagram for stars with 9 diblock arms, where  $\chi$  is the Flory–Huggins interaction parameter, N is the degree of polymerization of each arm, and  $f_{\rm A}$  is the volume fraction of the end blocks. The calculation is limited to the disordered (DIS) phase and the ordered lamellar (LAM), cylindrical (CYL), and bcc spherical (SPH) morphologies. The dotted line denotes the slice of the phase diagram studied in this paper.

a sample phase diagram for star block copolymers with M=9 arms. For the sake of simplicity, we ignore the complex gyroid and Fddd morphologies that exist in narrow channels between the LAM and CYL phases. Like all AB-type architectures, <sup>29</sup> the ordered phases extend down to a mean-field critical point, which is denoted by a solid dot in Figure 1. The fact that this does not happen in the SCFT phase diagram of ref 24 implies that their calculation suffers from a significant degree of numerical inaccuracy. This is not the case here; the spectral method provides superb accuracy.

In the previous simulations by Hart et al.,  $^{23}$  stars of different M were compared holding the total number of segments constant. As a result, they found large shifts in the order—disorder transition and the domain size as M was increased. It is well understood,  $^{29}$  that the appropriate comparison should be done with a fixed number of segments in each arm, which is why we define N to be the polymerization of a single arm rather than the entire molecule.

In our study, we examine the star blocks over compositions  $f_A$  < 0.5 at a fixed segregation of  $\chi N=30$  (denoted by the dotted line in Figure 1). Our attention is restricted to the left side of the phase diagram because thermoplastic elastomers require the glassy or semicrystalline domains to be discrete in order for the material to deform. Although one might expect that varying  $\chi N$  would have a significant effect on the bridging statistics due to the change in domain size, we know from strong-segregation theory that this is not the case. <sup>30</sup> Indeed, the previous SCFT calculations for linear ABA triblocks (i.e., M=2) <sup>4,5</sup> have shown that the bridging fraction becomes relatively insensitive to the value of  $\chi N$  once the melt is well segregated.

We begin by considering the simple LAM phase, where the only spatial dependence is with respect to the z coordinate normal to the lamellae. The A-segment concentration,  $\phi_{\rm A}(z)$ , for M=5 and 9 arm stars of composition  $f_{\rm A}=0.4$  is plotted

over one period (i.e., z = 0 to D) in Figures 2a and 2b, respectively, using a green dashed curve for the first cell (z < D/

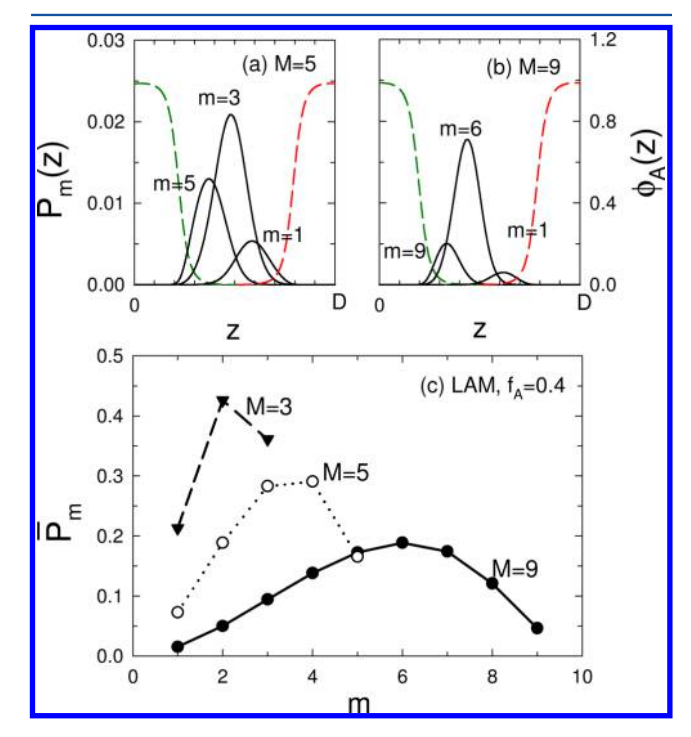


**Figure 2.** Bridging statistics for the LAM phase at  $\chi N=30$  and  $f_{\rm A}=0.4$ . The solid curves (scale on left) show the joint probability,  $P_m(z)$ , that an arm anchored in the first cell (|z| < D/2) belongs to a star centered at z with m of its (a) M=5 and (b) M=9 arms in the same cell. The A-segment profile,  $\phi_A(z)$ , is plotted with dashed curves (scale on right) using green in the first cell and red in the neighboring cell. Plot (c) shows the marginal distribution,  $\overline{P}_m$ , for the probability that an arm anchored in the first cell belongs to a star with m arms in that cell.

2) and a red dashed curve for the neighboring cell (z > D/2). The black solid curves show the joint probability,  $P_m(z)$ , that an arm anchored in the first cell belongs to a star with its center at z and m of its M arms in the same cell. In general, the maximum of  $P_m(z)$  occurs when m is a bit larger than M/2 and z is slightly shifted toward the first cell (i.e.,  $z \leq D/2$ ). It goes without saying that there is a strong correlation between z and m, since stars with their centers closer to a particular A domain are likely to have most of their arms in that domain.

The marginal distribution,  $\overline{P}_m$ , plotted in Figure 2c is obtained by integrating the area under each  $P_m(z)$  curve, and therefore it corresponds to the probability that an arm in the first cell belongs to a star with m arms in the first cell. In the LAM phase, a star with its center in a particular B lamella only ever has two A domains in which to anchor its arms. Hence, if we are told that a star has an arm anchored in the A domain of the first cell, it is likely that the center of the star is closest to that domain and in turn most of its arms are probably in the same domain. This is reflected by the fact that the peak in  $\overline{P}_m$  occurs at  $m \gtrsim M/2$ .

Next, we examine the CYL phase at a composition of  $f_A$  = 0.25. The joint distribution,  $P_m(\mathbf{r})$ , is now a function of the two spatial dimensions normal to the cylinder axis, which makes it more difficult to plot. Therefore, we restrict our attention to M = 9 stars and show two-dimensional density plots of  $P_m(\mathbf{r})$  for several values of m in Figures 3a-d. The circular curves denote the A/B interfaces (defined by  $\phi_A(\mathbf{r})$  = 0.5); the interface of the

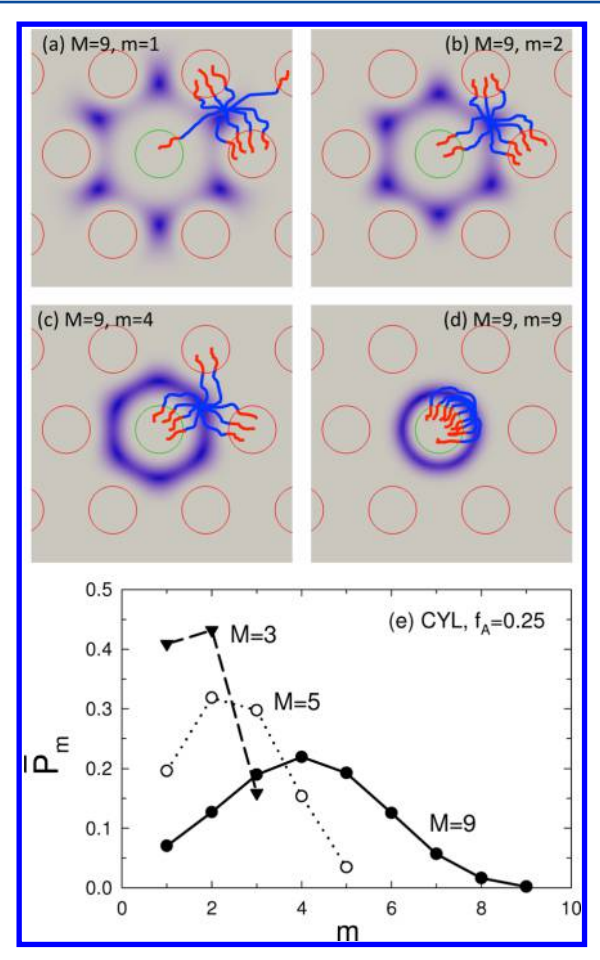


**Figure 3.** Similar plots to those of Figure 2, but for the CYL phase at  $\chi N=30$  and  $f_{\rm A}=0.25$ . The joint distribution,  $P_m({\bf r})$ , of a 9-arm star is shown with density plots (a) to (d) for different values of m. The A/B interfaces are plotted in green for the first cell and red for the other cells. A sample polymer configuration is illustrated in each plot. The marginal distribution,  $\overline{P}_{m}$  is given in plot (e).

first cell is shown in green, and others are plotted in red. When a star only has one arm in the first cell (i.e., m=1), its center tends to be located between a pair of neighboring A domains to which most of the remaining eight arms anchor, as illustrated by the typical configuration shown in Figure 3a. For larger values of m, the center of the star tends to locate closer to the A domain of the first cell. In Figure 3d, where all the arms are anchored in the first cell (i.e., m=M), the center of the star is confined to a circular annulus in close proximity to its A/B interface.

The marginal distribution,  $\overline{P}_m$ , for the CYL phase is plotted in Figure 3e for stars with M=3, 5, and 9 arms. In this case, the maximum in  $\overline{P}_m$  tends to occur at a smaller value of m than it did for the LAM phase. This is because there are positions in the B domain where the arms of the star can readily select between three different A domains. As such, the maximum tends to occur in the range  $M/3 \gtrsim m \gtrsim M/2$ .

Last, but not least, we examine the SPH phase at  $f_A = 0.16$ . In this case, the joint distribution is particularly difficult to visualize, given that it now depends on all three spatial dimensions. To deal with this, Figures 4a and 4b plot the level surface of  $P_m(\mathbf{r})$  at half its maximum for M = 9 stars with m = 1 and 2 arms anchored in the first cell, respectively. As before, the A/B interface of the first cell is shown in green, while those of

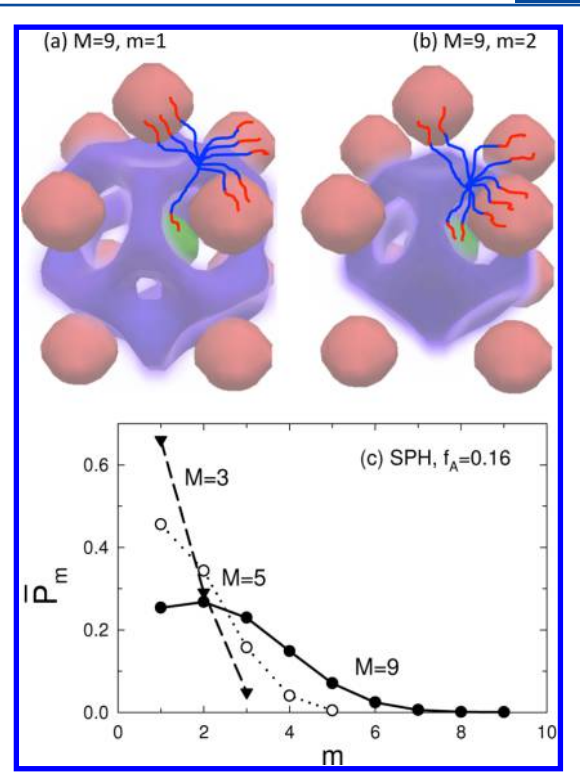


**Figure 4.** Similar plots to those of Figure 2, but for the SPH phase at  $\chi N = 30$  and  $f_A = 0.16$ . Level surfaces of the joint distribution,  $P_m(\mathbf{r})$ , of a 9-arm star are plotted in blue for (a) m = 1 and (b) m = 2. The A/B interfaces are plotted in green for the first cell and red for the other cells. A sample polymer configuration is illustrated in each plot. The marginal distribution,  $\overline{P}_{mv}$  is given in plot (c).

the other cells are shown in red. For stars with only one arm anchored in the first cell, their centers tend to be located well outside the cell where their remaining eight arms can readily anchor in the neighboring A domains. Again, as the number of arms in the first cell increases (e.g., m=2), the distribution  $P_m(\mathbf{r})$  becomes more localized around the A/B interface of the first cell.

The marginal probability,  $\overline{P}_m$ , for the SPH phase is shown in Figure 4c for stars with M=3, 5, and 9 arms. Since there are now locations in the B-rich matrix where the stars can simultaneously bridge to numerous different A domains, the maximum in  $\overline{P}_m$  occurs at a smaller value of m than it did for the LAM and CYL phases. The fact that  $\overline{P}_m$  for the M=9 arm stars is largest for  $m\approx 2$  implies that the stars are typically bridging between about four different A domains with roughly two arms in each of them.

To conclude, Figure 5 plots the fraction of stars,  $\nu_{\rm b}$ , that bridge between two or more domains as a function of composition,  $f_{\rm A}$ . As we should expect, the results for M=2 (i.e., linear ABA triblocks) match those of the previous SCFT method. In all cases, the bridging increases as the morphology changes from LAM to CYL to SPH. We can attribute this to the fact that the number of nearest-neighbor cells increases from two to six to eight, respectively, thus providing a greater opportunity for bridging. Not surprisingly, an increase in the number of arms, M, also enhances the bridging. It is noteworthy, though, how rapidly  $\nu_{\rm b}$  increases with M. By the time M=9, virtually all the stars form bridges in the CYL and SPH phases, the two morphologies best suited to thermoplastic elastomers.

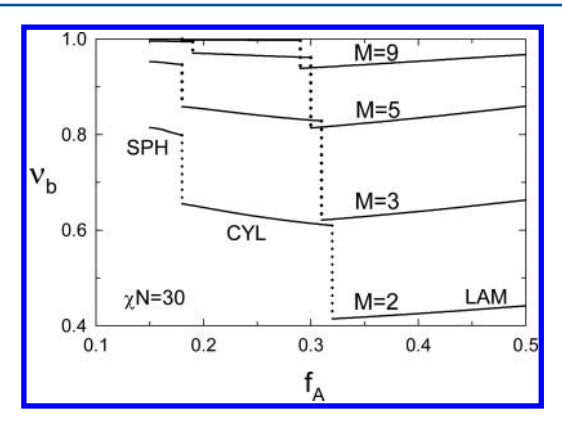


**Figure 5.** Bridging fractions,  $\nu_{\rm b}$ , as a function of the relative length of the end block,  $f_{\rm A}$ , plotted for stars with M=2, 3, 5, and 9 arms. Dotted lines denote discontinuous changes in  $\nu_{\rm b}$  at the order—order transitions between the LAM, CYL, and SPH phases.

#### DISCUSSION

The enhanced bridging predicted by SCFT offers a natural explanation for the observed improvement in mechanical properties of  $(AB)_M$  star blocks over those of ABA triblocks. One reason the bridging increases is that the centers of the stars (i.e., s=1) become more localized near the middle of the majority B domain. This follows from the fact that the concentration of the centers,  $\rho(\mathbf{r},1)=Vq^M(\mathbf{r},1)/Q$ , is proportional to a larger power of the partial partition function. In the simple LAM phase, for instance, the width of  $\rho(\mathbf{r},1)$  for 9-arm stars is reduced by 25% relative to that of ABA triblocks. Given that the stars have their centers nearer the middle of the B domain, their arms are less likely to favor any particular A domain.

The law of large numbers is another contributing factor to the higher bridging fraction. The probability of an arm, from a star with its center at  $\mathbf{r}$ , anchoring in the first cell is  $p = \overline{q}(\mathbf{r},1)/q(\mathbf{r},1)$ . Since the arms of a flexible star are statistically independent, the number of arms in the first cell will obey the binomial distribution. As such, the expected number of arms in the first cell,  $\langle m \rangle = Mp$ , is linear in M, whereas the standard deviation,  $\sigma_m = [Mp(1-p)]^{1/2}$ , only increases as the square root of M. The general consequence is that the arms will tend to be split more evenly among the accessible A domains, when M is larger.

Naturally, the fact that stars have multiple arms allows them to bridge between more than just two domains. In the CYL phase, there are positions in the middle of the B domain where the stars can readily bridge between three A-rich cylinders (see Figure 3b). In the SPH phase, the number of accessible A-rich domains increases to about four. This is evident in Figure 4c, where  $\overline{P}_m$  for M=9 stars has a maximum at m=2. This implies that the minority blocks in the first cell are most likely to belong to stars with only one other arm in that same A-rich sphere; the remaining seven arms are likely to be divided among several different spheres.

If so desired, one can readily extend the present approach to evaluate all kinds of joint distributions. For instance, by calculating partition functions for arms constrained to two different Voronoi cells,  $\overline{q}_1(\mathbf{r},s)$  and  $\overline{q}_2(\mathbf{r},s)$ , one could obtain the joint distribution,  $\overline{P}_{m_1,m_2}$ , for the probability that  $m_1$  arms are in cell one and  $m_2$  arms are in cell two, while the remaining  $M-m_1-m_2$  arms reside in other cells. It is just a matter of deciding what quantities provide useful information.

The previous SCFT method<sup>5,30</sup> for calculating bridging statistics is limited to architectures where both ends of a B block are constrained to the A/B interfaces. This restriction is nevertheless satisfied by many architectures, not just linear architectures but also the combs simulated in ref 23 and even the miktoarm star studied in refs 17, 18, and 19. The limitation of the method only arises when one end of the B block is free to move throughout the B domain, as is the case for the  $(AB)_M$  star or the more complex architectures recently studied in refs 15, 16, and 31. Our new method is able to handle these architectures as well as the ones of the previous method. In fact, when the architecture is symmetric about the center of the B block, as is the case for symmetric ABA triblocks, our approach is computationally faster because it only needs to integrate  $\overline{q}_1(\mathbf{r},s)$  over half the B block.

The attempt by Xu et al.<sup>24</sup> to extend the previous SCFT method applied the binomial distribution to the single-arm probability,  $p = \overline{q}(\mathbf{r},1)/q(\mathbf{r},1)$ , weighted by the distribution of the center of the star,  $\rho(\mathbf{r},1)$ . Although the binomial distribution applies to a star with a fixed center, it does not apply to the whole distribution of positions because m and  $\mathbf{r}$  are correlated. The evaluation of joint or conditional probabilities can sometimes be counterintuitive, and so the evaluation of bridging statistics requires considerable care.

Simulations offer a more straightforward way of evaluating bridging statistics than SCFT, but they are far more computationally costly. While simulations have progressed enormously over recent years to the point where they can handle simple architectures like the AB diblock and ABA triblock copolymers with relative ease, complex architectures involving a large number of blocks still pose a daunting computational challenge. Indeed, the bead—spring model of the M=6 arm star block simulated by Hart et al. was limited to merely four beads per B block. Even then, their evaluation of  $\nu_{\rm b}$  was limited to the simple LAM phase. In contrast, our SCFT calculation takes mere seconds to determine the equilibrium phase and evaluate the bridging statistics regardless of the morphology.

Only time will tell, but  $(AB)_M$  star blocks may eventually become an architecture of choice for thermoplastic elastomers. They have been studied for decades,  $^{32-38}$  and there are now straightforward synthetic techniques for tuning the number of arms. Undoubtedly, there will be various ways of improving their performance as thermoplastic elastomers. For instance, the compositional shift in the morphologies that has been attributed to the superior performance of miktoarm star blocks  $^{17-19}$  could be realized in this system by, for example, introducing polydispersity into the A blocks. However, the resulting advantage of larger minority domains will have to be balanced against the increased probability of short A blocks pulling out their domains. With the added capability of evaluating the bridging statistics, SCFT will be a great asset in exploring such modifications to the system.

#### SUMMARY

A new versatile and computationally efficient SCFT method has been devised for calculating the bridging statistics of complex block copolymer architectures. The method was applied to melts of  $(AB)_M$  stars, each consisting of M identical diblock arms. As is the case for linear ABA triblock copolymers (i.e., M=2), the fraction of molecules,  $\nu_b$ , that bridge between discrete A domains increases as the morphology changes from lamellar (LAM) to cylindrical (CYL) to bcc spherical (SPH).

However, the propensity to bridge between minority domains is greater for stars than triblocks, especially as the number of arms is increased. In fact, virtually all star molecules form bridges once  $M \gtrsim 10$ . Some of the improvement can be attributed to the greater tendency of stars to locate in the center of the B domain, where the arms have a balanced access to multiple A-rich domains. More importantly, stars with many arms benefit from the law of large numbers, which favors an equal partitioning of arms among the available domains.

The superior bridging statistics of  $(AB)_M$  stars relative to the simpler ABA triblocks provides an explanation for the improved mechanical properties observed in experiment. Given the well-developed synthetic techniques, diblock-arm stars should offer a viable way of improving the performance of thermoplastic elastomers. There will undoubtedly be scope for modifications to the architecture, such as polydispersity in the end blocks, that could further improve the properties. The existing SCFT algorithms for efficiently predicting the phase behavior of complex block copolymer architectures coupled with our new method of evaluating bridging statistics will undoubtedly provide valuable guidance for optimizing this system as well as ones based on other complex architectures like those recently studied by refs 15, 16, and 31.

#### AUTHOR INFORMATION

#### **Corresponding Authors**

\*E-mail: r6spence@uwaterloo.ca (R.K.W.S.).

\*E-mail: mwmatsen@uwaterloo.ca (M.W.M.).

# ORCID ®

Mark W. Matsen: 0000-0003-2099-0892

#### **Notes**

The authors declare no competing financial interest.

# ACKNOWLEDGMENTS

This work was funded by the NSF through the Center for Sustainable Polymers (CHE-1413862).

# REFERENCES

- (1) Bates, C. M.; Bates, F. S. 50th Anniversary Perspective: Block Polymers Pure Potential. *Macromolecules* **2017**, *50*, 3–22.
- (2) Watanabe, H. Slow Dielectric Relaxation of a Styrene-Isoprene-Styrene Triblock Copolymer with Dipole Inversion in the Middle Block: A Challenge to a Loop/Bridge Problem. <u>Macromolecules</u> 1995, 28, 5006—5011.
- (3) Karatasos, K.; Anastasiadis, S. H.; Pakula, T.; Watanabe, H. On the Loops-to-Bridges Ratio in Ordered Triblock Copolymers: An Investigation by Dielectric Relaxation Spectroscopy and Computer Simulations. *Macromolecules* **2000**, *33*, 523–541.
- (4) Matsen, M. W.; Schick, M. Lamellar Phase of a Symmetric Triblock Copolymer. *Macromolecules* **1994**, *27*, 187–192.
- (5) Matsen, M. W.; Thompson, R. B. Equilibrium Behavior of Symmetric ABA Triblock Copolymer Melts. *I. Chem. Phys.* 1999, 111, 7139–7146.
- (6) Spontak, R. J.; Smith, S. D. Perfectly-Alternating Linear (AB)<sub>n</sub> Multiblock Copolymers: Effect of Molecular Design on Morphology and Properties. *I. Polym. Sci., Part B: Polym. Phys.* **2001**, 39, 947–955.
- (7) Hermel, T. J.; Hahn, S. F.; Chaffin, K. A.; Gerberich, W. W.; Bates, F. S. Role of Molecular Architecture in Mechanical Failure of Glassy/Semicrystalline Block Copolymers:? CEC vs CECEC Lamellae. <u>Macromolecules</u> 2003, 36, 2190–2193.
- (8) Koo, C. M.; Hillmyer, M. A.; Bates, F. S. Structure and Properties of Semicrystalline-Rubbery Multiblock Copolymers. <u>Macromolecules</u> **2006**, *39*, 667–677.

(9) Matsumiya, Y.; Watanabe, H.; Takano, A.; Takahashi, Y. Uniaxial Extensional Behavior of (SIS)<sub>p</sub>. Type Multiblock Copolymer Systems: Structural Origin of High Extensibility. <u>Macromolecules</u> **2013**, 46, 2681–2695.

- (10) Drolet, F.; Fredrickson, G. H. Optimizing Chain Bridging in Complex Block Copolymers. *Macromolecules* **2001**, *34*, 5317–5324.
- (11) Rasmussen, K. Ø.; Kober, E. M.; Lookman, T.; Saxena, A. Morphology and Bridging Properties of (AB)<sub>n</sub> Multiblock Copolymers. *J. Polym. Sci., Part B: Polym. Phys.* **2003**, *41*, 104–111.
- (12) Shah, M.; Ganesan, V. Chain Bridging in a Model of Semicrystalline Multiblock Copolymers. *J. Chem. Phys.* **2009**, *130*, 054904
- (13) Mays, J. W.; Uhrig, D.; Gido, S.; Zhu, Y.; Weidisch, R.; Iatrou, H.; Hadjichristidis, N.; Hong, K.; Beyer, F.; Lach, R.; Buschnakowski, M. Synthesis and Structure Property Relationships for Regular Multigraft Copolymers. *Macromol. Symp.* **2004**, *215*, 111–126.
- (14) Jiang, F.; Wang, Z.; Qiao, Y.; Wang, Z.; Tang, C. A Novel Architecture toward Third-Generation Thermoplastic Elastomers by a Grafting Strategy. *Macromolecules* **2013**, *46*, 4772–4780.
- (15) Zhang, J.; Li, T.; Mannion, A. M.; Schneiderman, D. K.; Hillmyer, M. A.; Bates, F. S. Tough and Sustainable Graft Block Copolymer Thermoplastics. *ACS Macro Lett.* **2016**, *5*, 407–412.
- (16) Zhang, J.; Schneiderman, D. K.; Li, T.; Hillmyer, M. A.; Bates, F. S. Design of Graft Block Polymer Thermoplastics. <u>Macromolecules</u> **2016**, 49, 9108–9118.
- (17) Lynd, N. A.; Oyerokun, F. T.; O'Donoghue, D. L.; Handlin, D. L.; Fredrickson, G. H. Design of Soft and Strong Thermoplastic Elastomers Based on Nonlinear Block Copolymer Architectures Using Self-Consistent-Field Theory. *Macromolecules* **2010**, *43*, 3479–3486.
- (18) Shi, W.; Lynd, N. A.; Montarnal, D.; Luo, Y.; Fredrickson, G. H.; Kramer, E. J.; Ntaras, C.; Avgeropoulos, A.; Hexemer, A. Toward Strong Thermoplastic Elastomers with Asymmetric Miktoarm Block Copolymer Architectures. *Macromolecules* **2014**, *47*, 2037–2043.
- (19) Shi, W.; Hamilton, A. L.; Delaney, K. T.; Fredrickson, G. H.; Kramer, E. J.; Ntaras, C.; Avgeropoulos, A.; Lynd, N. A.; Demassieux, Q.; Creton, C. Aperiodic "Bricks and Mortar" Mesophase: a New Equilibrium State of Soft Matter and Application as a Stiff Thermoplastic Elastomer. <u>Macromolecules</u> 2015, 48, 5378–5384.
- (20) Puskas, J. E.; Antony, P.; el Fray, M.; Altstädt, V. The Effect of Hard and Soft Segment Composition and Molecular Architecture on the Morphology and Mechanical Properties of Polystyrene-Polyisobutylene Thermoplastic Elastomeric Block Copolymers. *Eur. Polym. J.* 2003, *39*, 2041–2049.
- (21) Kong, J. F.; Lipik, V.; Abadie, M. J. M.; Deen, G. R.; Venkatraman, S. S. Characterization and Degradation of Elastomeric Four-Armed Star Copolymers Based on Caprolactone and L-Lactide. *I. Biomed. Mater. Res., Part A* **2012**, *100A*, 3436–3445.
- (22) Burns, A. B.; Register, R. A. Mechanical Properties of Star Block Polymer Thermoplastic Elastomers with Glassy and Crystalline End Blocks. *Macromolecules* **2016**, *49*, 9521–9530.
- (23) Hart, K. E.; Abbott, L. J.; Lísal, M.; Colina, C. M. Morphology and Molecular Bridging in Comb- and Star-Shaped Diblock Copolymers. *I. Chem. Phys.* **2014**, *141*, 204902.
- (24) Xu, Y.; Li, W.; Qiu, F.; Lin, Z. Self-Assembly of 21-Arm Star-Like Diblock Copolymer in Bulk and Under Cylindrical Confinement. *Nanoscale* **2014**, *6*, 6844–6852.
- (25) Matsen, M. W. The Standard Gaussian Model for Block Copolymer Melts. *J. Phys.: Condens. Matter* **2002**, *14*, R21–R47.
- (26) Matsen, M. W.; Schick, M. Microphase Separation in Starblock Copolymer Melts. <u>Macromolecules</u> **1994**, *27*, *6761–6767*.
- (27) Matsen, M. W. Fast and Accurate SCFT Calculations for Periodic Block-Copolymer Morphologies using the Spectral Method with Anderson Mixing. *Eur. Phys. I. E: Soft Matter Biol. Phys.* **2009**, *30*, 361–369.
- (28) Ranjan, A.; Qin, J.; Morse, D. C. Linear Response and Stability of Ordered Phases of Block Copolymer Melts. <u>Macromolecules</u> 2008, 41, 942–954.

(29) Matsen, M. W. Effect of Architecture on the Phase Behavior of AB-Type Block Copolymer Melts. <u>Macromolecules</u> **2012**, *45*, 2161–2165.

- (30) Matsen, M. W. Bridging and Looping in Multiblock Copolymer Melts. *I. Chem. Phys.* **1995**, *102*, 3884–3887.
- (31) Mannion, A. M.; Bates, F. S.; Macosko, C. W. Synthesis and Rheology of Branched Multiblock Polymers Based on Polylactide. <u>Macromolecules</u> **2016**, 49, 4587–4598.
- (32) Bi, L.-K.; Fetters, L. J. Synthesis and Properties of Block Copolymers. 3. Polystyrene-Polydiene Star Block Copolymers. Macromolecules 1976, 9, 732–742.
- (33) Alward, D. B.; Kinning, D. J.; Thomas, E. L.; Fetters, L. J. Effect of Arm Number and Arm Molecular Weight on the Solid-State Morphology of Poly(styrene-isoprene) Star Block Copolymers. <u>Macromolecules</u> 1986, 19, 215–224.
- (34) Herman, D. S.; Kinning, D. J.; Thomas, E. L.; Fetters, L. J. A Compositional Study of the Morphology of 18-Armed Poly(styrene-isoprene) Star Block Copolymers. <u>Macromolecules</u> 1987, 20, 2940–2942.
- (35) Hashimoto, T.; Ijichi, Y.; Fetters, L. J. Order-Disorder Transition of Starblock Copolymers. *J. Chem. Phys.* **1988**, 89, 2463–2472.
- (36) Uchida, S.; Ichimura, A.; Ishizu, K. Preparation and Microphase-Separated Structures of  $(AB)_n$  Star-Block Copolymers Composed of Symmetric Diblock Arms. <u>Polymer</u> **1999**, 40, 1019–1023.
- (37) Jang, S.; Moon, H. C.; Kwak, J.; Bae, D.; Lee, Y.; Kim, J. K.; Lee, W. B. Phase Behavior of Star-Shaped Polystyrene-block-poly-(methylmethacrylate) Copolymers. <u>Macromolecules</u> **2014**, 47, 5295–5302.
- (38) Park, J.; Jang, S.; Kim, J. K. Morphology and Microphase Separation of Star Copolymers. <u>I. Polym. Sci. Part B: Polym. Phys.</u> **2015**, 53, 1–21.